Japanese Journal of Applied Physics

RAPID COMMUNICATION

Influence of heterostructure on structure, electric and magnetic properties of $Bi_{0.5}(Na_{0.80},K_{0.20})_{0.5}TiO_3/BaZrO_3$ films prepared by the sol–gel method

To cite this article: Ngo Duc Quan *et al* 2023 *Jpn. J. Appl. Phys.* **62** 040901

Japanese Journal of Applied Physics **62**, 040901 (2023) **RAPID COMMUNICATION**
https://doi.org/10.35848/1347-4065/acc5c7

Influence of heterostructure on structure, electric and magnetic properties of $Bi_{0.5}(Na_{0.80},K_{0.20})_{0.5}TiO_3/BaZrO_3$ films prepared by the sol–gel method

Ngo Duc Quan[1*], Pham Van Tuan[2], Nguyen Duc Minh[3], and Guus Rijnders[3]

[1]School of Engineering Physics, Hanoi University of Science and Technology, No.1 Dai Co Viet, Hanoi 100000, Vietnam
[2]International Training Institute for Materials Science, Hanoi University of Science and Technology, No.1 Dai Co Viet, Hanoi 100000, Vietnam
[3]MESA + Institute for Nanotechnology, University of Twente, PO Box 217, 7500AE Enschede, The Netherlands

*E-mail: quan.ngoduc@hust.edu.vn

Received November 9, 2022; revised March 8, 2023; accepted March 19, 2023; published online April 12, 2023

This study reports on the structure, electric, and magnetic properties of $Bi_{0.5}(Na_{0.80},K_{0.20})_{0.5}TiO_3/BaZrO_3$ (BNKT/BZO) heterolayered films synthesized via chemical solution deposition on Pt/Ti/SiO_2/Si substrates. The influence of different heterolayered configurations on the microstructure, electric and magnetic properties of the films was investigated thoroughly. The heterostructures are expected to generate strongly correlated electron systems in the BNKT and BZO layers that cause a magnetic interface effect in the BNKT/BZO conjunction layer. The BZO layer also prevents metal ion evaporation, resulting in a decline in oxygen vacancies and an enhancement in the electric and magnetic properties. The obtained results show that magnetic properties and leakage current density (J) of BNKT/BZO heterolayered films were greatly improved thanks to the heterolayered structure. Heterolayered 4BNKT/2BZO films (M42) yield the highest M_s and M_r values of 14.4 emu cm^{-3} and 1.7 emu cm^{-3}, respectively, about three times higher than multilayered BNKT. Thanks to heterolayered structure, J decreases strongly from 16.0 $\times$ 10^{-4} A cm^{-2} for BNKT films to 1.4 $\times$ 10^{-4} A cm^{-2} for heterolayered M42 films. It has been verified that the leakage current in BNKT/BZO heterolayered films follows the Schottky barrier mechanism, with the barrier height fluctuating between 0.80 eV and 0.92 eV. The results of the study show that BNKT/BZO heterolayered films may be suitable for use in environmentally friendly multifunction devices. © 2023 The Japan Society of Applied Physics

Currently, multiferroics, which can simultaneously exhibit magnetic, electrical or elastic phases, are being extensively introduced for applications in modern life and technology. Such systems are exploited for applications such as AC magnetic field sensors with high sensitivity, electromagnetic-tuned ultrasonic generators, or filters, transducers or phase shifters in which the magnetic resonance properties (ferromagnetic, ferrimagnetic, antiferromagnetic etc.) are controlled by the electric field instead of the magnetic field.[1)] Multiferroics has been studied since the 1960s.[2)] However, it received little attention and only became really vibrant from 2003 with the discovery of large polarization in $BiFeO_3$ epitaxial thin films[3)] and strong electromagnetic coupling in $TbMnO_3$[4)] and $TbMn_2O_5$.[5)] Later, more and more potential multiferroics were discovered and studied in detail, such as ferroelectric–ferromagnetic composites (nickel ferrite–PZT and manganite–PZT; PZT = $Pb(ZrTi)O_3$).[6)] Gao and co-workers reported an approach to control and switch the ferromagnetic orientation with an electric field using multiferroic $Ni_{0.5}Zn_{0.5}Fe_2O_4$@$CoFe_2O_4$ fluids with core–shell structured particles.[7)] A new magnetoelectric multiferroic fluid has recently been reported. It is made from composite nanoparticles of $BaTiO_3$@$CoFe_2O_4$, which are dispersed in a non-polar and highly insulating mixture of oleic acid and silicone oil.[8)] A recently published article states that $Co_{0.6}Cu_{0.3}Zn_{0.1}Fe_2O_4/Ba_{0.9}Sr_{0.1}Zr_{0.1}Ti_{0.9}O_3$ ceramic, a high-performing multiferroic composite, has demonstrated improved magnetoelectric coupling effects.[9)] Nevertheless, lead-based PZT materials and its composites are the traditional multiferroics that are widely handled in consumer or industrial systems. PZT shows stable and excellent properties, and is likely to form composites with ferromagnetics, such as $CoFe_2O_4$, to produce multiferroics.[10)] However, such systems are responsible for environmental pollution and harm to human health because they contain a large amount of toxic lead.[11)] Hence, lead-free multiferroics have attracted increasing attention.[12)] Among lead-free materials, the Bi(Na,Ka)TiO3 (BNKT) system is thought to be a potential candidate and likely replacement for PZT, because similar to Pb^{2+}, Bi^{3+} ions possess strong polarizability.[13)] Earlier studies showed that BNKT compounds at the morphotropic phase boundary (MPB) reveal excellent electromechanical behaviors and coupling.[14)] Their key properties such as remnant polarization (Pr $\sim$ 38 μC cm^{-2}), piezoelectric coefficient (d_{33} $\sim$ 167 pC N^{-1}) or electromechanical coupling coefficient (k_{33} $\sim$ 0.56) are able to compare with those of PZT.[15)] In particular, Wang et al discovered that BNKT systems have RT ferromagnetic order, although it is of low intensity and its mechanism is not obvious yet.[16)] Forming multiferroics based on composite BNKT materials has been proposed as an effective solution to this problem.[17,18)] Some configurations of multiferroic composites (such as particles mixed in a matrix, laminated bilayers, homogeneous mixtures, laminated multilayers or fiber multiferroic composites) were reported to possess a magnetic–electric behavior numerous orders of amplitude higher than single-phase multiferroics. Moreover these allow flexible selection of the electric and magnetic orders to control properties matching with specific applications. The literature available on BNKT multiferroics exposes certain gaps that need to be addressed. Firstly, the introduction of a magnetic phase into a ferroelectric/piezoelectric one can lead to a decrease in mechanical–electric properties and an increase in the complexity of preparation processes.[18–20)] Secondly, J possesses a relatively high value. Furthermore, there is currently no clear understanding of the mechanism behind the multiferroic properties of BNKT. In this report, by chemical solution deposition, BNKT multiferroic films with heterostructures can be easily synthesized and their characteristics such as composition, stoichiometry, thickness, grain boundaries and crystalline structure can be managed with a greater degree of precision.[21)] The heterostructures are expected to generate strongly correlated electron systems in BNKT and BZO layers that cause a magnetic interface effect in the BNKT/BZO conjunction layer. The BZO layer also prevents metal ion evaporation, resulting in a decline in oxygen vacancies and an enhancement of electric and magnetic properties.

In this report, the influence of the heterostructure between $Bi_{0.5}(Na_{0.80},K_{0.20})_{0.5}TiO_3$ (BNKT) and $BaZrO_3$ (BZO) on the structure, electrical and magnetic properties of $Bi_{0.5}(Na_{0.80},K_{0.20})_{0.5}TiO_3/BaZrO_3$ (BNKT/BZO) films is investigated. This study aims to improve electric and magnetic properties by pursuing the following objectives: (i) creating a heterostructure that induces strongly correlated electron systems within BNKT and BZO layers, leading to a magnetic interface effect in the BNKT/BZO conjunction layer; (ii) utilizing the BZO layer to prohibit metal ion evaporation and consequently reduce oxygen vacancies; (iii) causing competition and interaction between the symmetry of BZO and of BNKT. The obtained results show that both the electrical and magnetic properties of the films changed with the thickness of the individual films and achieved the highest values thanks to this heterolayer structure. The nature of these improvements in the electrical and magnetic properties will be elucidated later.

The multilayered BZO and BNKT and heterolayered BNKT/BZO films were formed on $Pt/Ti/SiO_2/Si$ substrates using solutions prepared by a sol–gel technique. Here, the BZO precursor solution was prepared from barium acetate $[(CH_3COO)_2Ba]$ and zirconium *n*-propoxide $(Zr[n\text{-}OPr]_4)$ in 2-methoxyethanol solvent. The BNKT precursor solution is derived from sodium nitrate ($NaNO_3$), potassium nitrate (KNO_3), bismuth nitrate $[Bi(NO_3)_3{\cdot}5H_2O]$ and titanium isopropoxide $(Ti[i\text{-}OPr]_4)$ in 2-methoxyethanol solvent.[22] Each layer of the BNKT/BZO films was formed by spin coating 0.4 M precursor on substrates at 4000 rpm for 30 s, followed by pyrolysis at 400 °C for 10 min. The process was repeated until BNKT/BZO films with a total of six coating layers were obtained. Finally, thermal annealing at 700 °C for 60 min was carried out to obtain the ferroelectric phase in the BNKT/BZO thin films. Schematic diagrams of BZO and BNKT multilayered films and BNKT/BZO heterolayered films with a total of six coating layers in this study are shown in Fig. 1, wherein [mBNKT/nBZO] heterolayered films are denoted as M11 ($m = 1$, $n = 1$), M22 ($m = 2$, $n = 2$), M33 ($m = 3$, $n = 3$) and M42 ($m = 4$, $n = 2$).

Then measurements of the film characteristics were conducted. We used a field emission scanning electron microscope (FE-SEM; Hitachi S4800) to analyze the cross-sectional and surface morphologies of the films. The crystal behaviors of heterolayered BNKT/BZO films were characterized with a Bruker D5005 diffractometer (Ni-filtered and Cu Kα radiation, $\lambda = 1.5406$ Å, step of 0.02°, voltage of 45 kV and current of 40 mA). Electrical properties were measured with a TF Analyzer 2000 ferroelectric tester (aixACCT Systems GmbH, Germany), under applied voltages ranging from −25 V to 25 V and a frequency of 1000 Hz. The magnetic behaviors were characterized using a vibrating sample magnetometer (VSM; 7404, Lake Shore, USA).

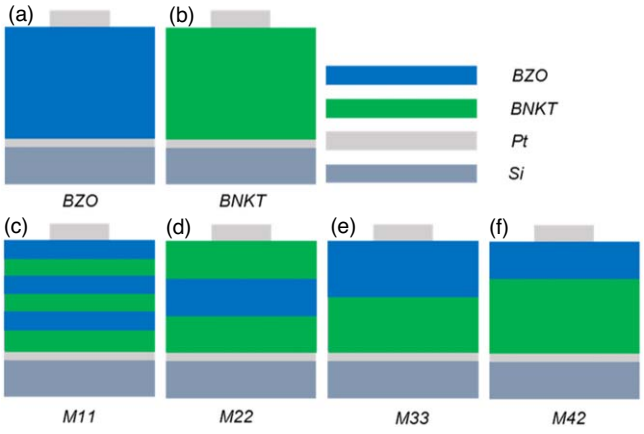

Fig. 1. Schematic diagrams of multilayered films with six coating layers: (a) BZO and (b) BNKT films and (c)–(f) BNKT/BZO heterolayered films with a total of six coating layers. [mBNKT/nBZO]: M11 ($m = 1$, $n = 1$), M22 ($m = 2$, $n = 2$), M33 ($m = 3$, $n = 3$) and M42 ($m = 4$, $n = 2$).

The surface morphologies of the BNKT/BZO heterolayered films were evaluated using FE-SEM images. Figure 2 shows the SEM images for BNKT/BZO heterolayered films. It is observed that films reveal a granular structure, specific for the films synthesized by the sol–gel technique, without signs of cracks. Grains possess a polyhedral shape and are of various sizes. Based on SEM images, the grain size of the films is estimated to be around 30 nm. The surface of films shows pores formed by the evaporation of the organic component during sintering at high temperatures. Film thicknesses are determined by cross-sectional SEM images and are about 400 nm as shown in Fig. 2(f). The rms value of the films, a necessary parameter to evaluate the quality of the films, was determined via atomic force microscopy (AFM) analysis. This parameter is obtained by software in the AFM equipment and is shown in Table I. It is relatively small and fluctuates from 10.2 nm to 15.5 nm. Such small rms values confirm that the prepared films exhibit good surface quality.

XRD spectra of the Si-Pt/BNKT/BZO heterostructure films are demonstrated in Fig. 3. As observed, heterostructure films reveal the diffraction peaks belonging to the bi-phase perovskite structures of BNKT and BZO materials. No traces of strange phases are observed. The XRD patterns could be indexed based on JCPDS card no. 06-0399 of a cubic structure (Pm $\bar{3}$ m) for the BZO phase[23] and JCPDS card no. 04-011-3919 of a perovskite structure for the BNKT phase,[24] respectively. The (111) orientation, with the highest intensity, is contributed by the Pt-coated substrate. Figure 3(b) shows X-ray diffraction patterns of films magnified in the 2θ ranges of 30°–48°. The phase structure of BNKT multilayer film is typified by the peaks (marked by a $ sign), as (110) at around 32° and (200) at around 47°. This observation matches with previous works,[13,22] which reported that BNKT films possess an MPB component with rhombohedral and tetragonal symmetries. The cubic structure of BZO film shows the characteristic peaks (marked by a @ sign) as (100) at 30° and (200) at 43°.[23] For the heterostructure film M11, the diffraction peaks are relatively low, proving that the crystallization is poor. The diffraction peaks of the bi-phase perovskite structures in BNKT and BZO layers are observed more obviously for the samples M22, M33 and M42. The heterostructure M33 yields the best-crystallized characteristic with the diffraction peaks being high and sharp. The average crystalline sizes of films calculated using the Scherrer equation is $D = K\lambda/\beta\cos(\theta)$ via the XRD data. Where constants as D, K, λ, β and θ are the grain size, Scherrer constant (theoretically, K is equal to 0.9), wavelength, FWHM and Bragg angle, respectively. The D value illustrated in Table I fluctuated moderately from 31.5 to

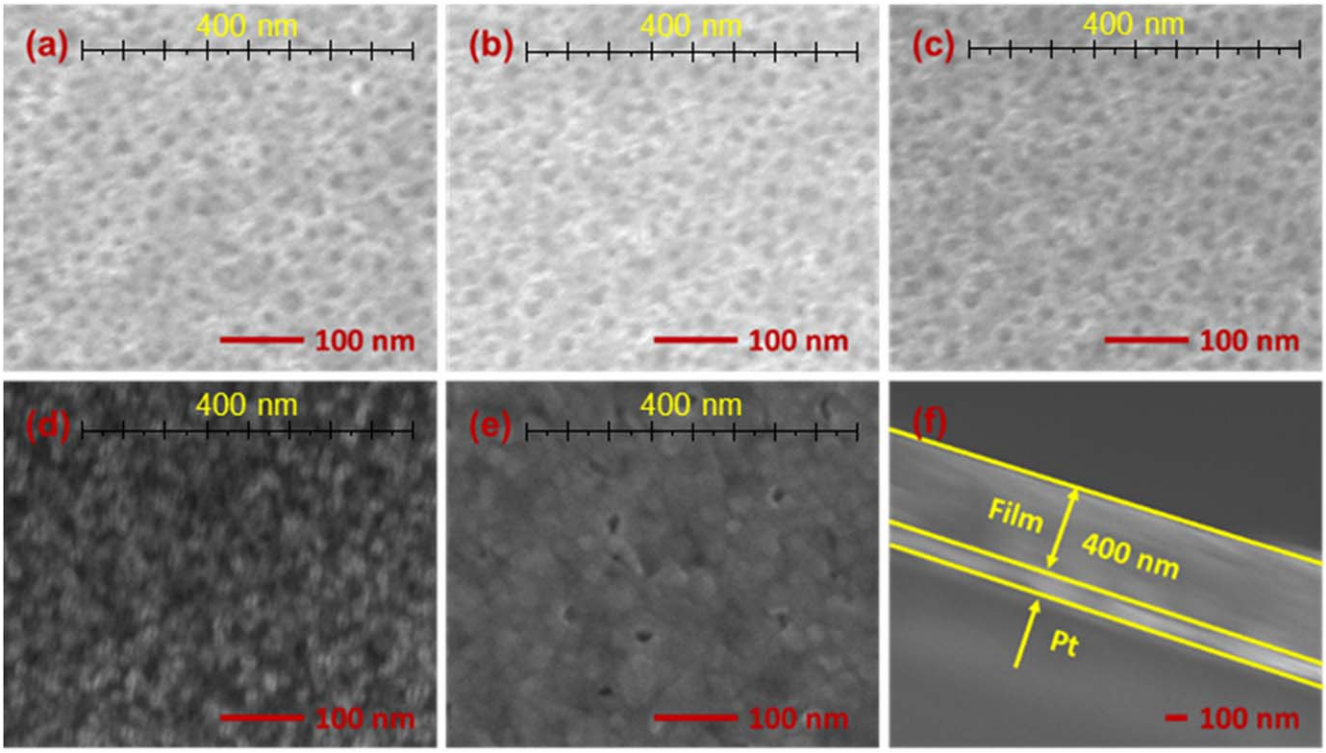

Fig. 2. SEM micrographs of samples: (a) M11, (b) M22, (c) M33, (d) M42, (e) BZO. (f) Cross-sectional SEM image of sample M11.

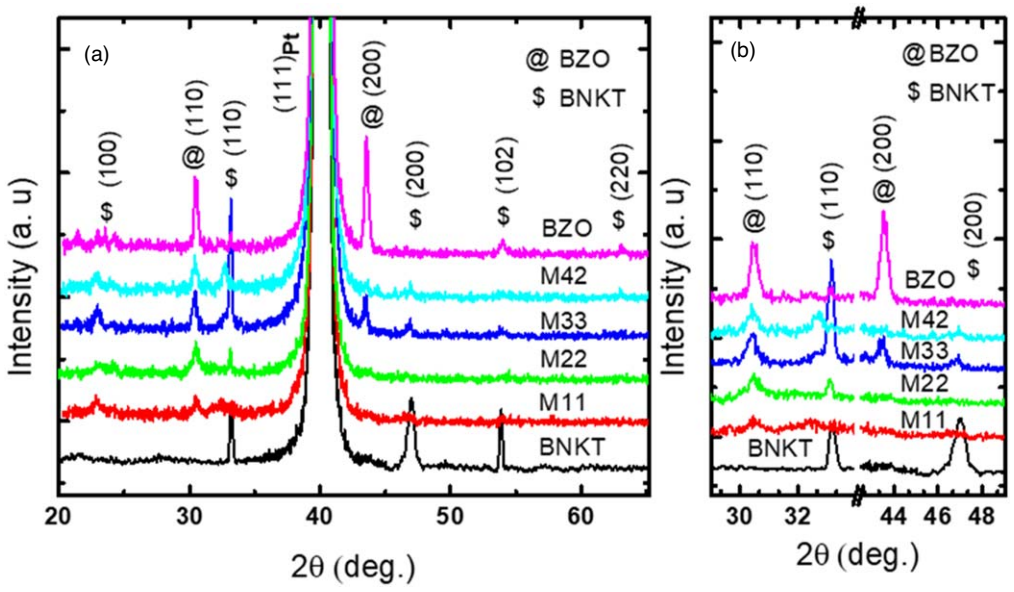

Fig. 3. (a) X-ray diffraction patterns of BNKT/BZO heterolayered films in the 2θ ranges of 20°–65°. (b) X-ray diffraction patterns in the 2θ ranges of 30°–48°.

Table I. Values of saturation magnetization (M_s), remnant magnetization (M_r), coercivity (H_c), leakage current density (J), root-mean-square (rms) and grain size (D) of BNKT/BZO films.

Sample	M_r (emu cm^{-3})	M_s (emu cm^{-3})	H_c (Oe)	J (A cm^{-2})	rms (nm)	D (nm)
BNKT	0.9	5.6	65	16.0×10^{-4}	10.7	33.1
M11	1.3	6.3	86	10.0×10^{-4}	10.2	31.5
M22	1.4	6.9	88	6.0×10^{-4}	11.6	32.7
M33	1.5	9.2	97	4.0×10^{-4}	15.1	33.3
M42	1.7	14.4	67	1.4×10^{-4}	14.0	32.8
BZO	1.3	9.9	59	1.0×10^{-4}	15.5	33.6

33.6 nm. It is matched with the grain size being observed from SEM images above.

Figure 4 demonstrates the RT magnetic hysteresis loops (*M–H*) for BNKT/BZO films: (a) under a magnetic field from −5 kOe to 5 kOe and (b) in the range of low magnetic fields from −1000 Oe to 1000 Oe. The multilayer BNKT films exhibit antiferromagnetic behaviors at RT that are proved via the magnetic hysteresis (*M–H*) loops belonging to the anti-S-shape type. This is attributed to the interaction between ferromagnetic and antiferromagnetic orders. The result is consistent with our previous study which investigated the effect of $BiFeO_3$ perovskite on the magnetic properties of lead-free BNKT films.[18] Similar behavior was also observed in BNT materials by Hung and co-workers.[25] It is believed that the antiferromagnetic properties in BNKT are contributed by the direct exchange coupling of Ti^{4+}–O–Ti^{4+} and/or the 3d° empty state of Ti^{4+}.[26] In contrast, multilayer BZO films show superparamagnetism at RT with the S-shaped magnetic hysteresis (*M–H*) loops being saturated and thin. This is in good agreement with work by Bakeer et al.[27] reporting that BZO materials show superparamagnetism at RT. Superparamagnetic behavior is contributed by oxygen vacancies formed during high sintering temperatures[28] or the interstitial arrangement of zirconium ions on the crystal lattice.[29] When being designed with the heterostructure configuration, the magnetic behaviors of BNKT/BZO heterolayered films change from antiferromagnetism for BNKT multilayered films to ferromagnetism for the heterolayered film M42. This transition is manifested by the gradual transformation of *M–H* loops from the anti-S-shape to the S-shape. Magnetic properties are also enhanced remarkably thanks to the heterolayered design. Values of saturation magnetization (M_s), remnant magnetization (M_r) and coercivity (H_c) were determined and are listed in Table I. M_r values are relatively small from 0.9 emu cm^{-3} to 1.7 emu cm^{-3} and the same is true of H_c from 59 Oe to 97 Oe. In contrast, M_s possesses high values from 5.6 emu cm^{-3} to 14.4 emu cm^{-3}. The insert in Fig. 4(a) shows the difference in M_s and M_r values between the heterolayered films. This indicates obviously that the heterolayered film M42 yields the highest M_s and M_r values of 14.4 emu cm^{-3} and 1.7 emu cm^{-3}, respectively. These values are superior to those of other films, and are about three times higher than for multilayered BNKT. This enhancement may be derived from strongly correlated electron systems in BNKT and BZO layers that cause a magnetic interface effect in BNKT/BZO heterostructures. At the interface of BNKT and BZO, direct exchange and superexchange will be reformed by the different ionic radii of Bi^{3+} and Ba^{2+} or Ti^{4+} and Zr^{4+} or strain causing altered bonding angles and bonding lengths. The BZO layer deposited on BNKT affects the magnetism of the heterolayered films by the residual strain which occurs at the BNKT/BZO interface, as has been published for $CoFe_2O_4$-PZT bilayers.[30] An additional possibility for the relative the improvement in ferromagnetism is intermixing of the BNKT and BZO at the interface layer. Koohfar and co-workers also reported similar behaviors in thin $La_{0.7}Sr_{0.3}Cr_{0.3}/La_{0.7}Sr_{0.3}MnO_3$ heterostructures.[31]

Leakage current density (*J*) is attributed to be a key parameter reflecting the quality and reliability of multiphase composite films. *J* measurements for the BNKT/BZO heterostructure films have been implemented at room temperature and Fig. 5(a) shows the obtained results. It is observed that films show low *J* values of below 10^{-4} A cm^{-2} at a low electric field (<100 kV cm^{-1}), and these values rise strongly with increase in the electric field. Figure 5(b) demonstrates the comparison of *J* values between the films measured at an electric field of 300 kV cm^{-1}. For the BNKT sample, *J* possesses a relatively high value of around 16.0×10^{-4} A cm^{-2}. It tends to decrease strongly in the M11, M22, M33, M42 films and BZO, respectively. Previous studies reported that the limitation of the transposition of charge carriers at the interfaces between different layers is responsible for the deduction in leakage current.[32] Minh and his co-workers[33] supposed that each interface reduces the probability that a potential leakage path reaches the outer electrodes. As a result, when the number of interface layers *N* increases the leakage current is observed to drop strongly. We suppose that

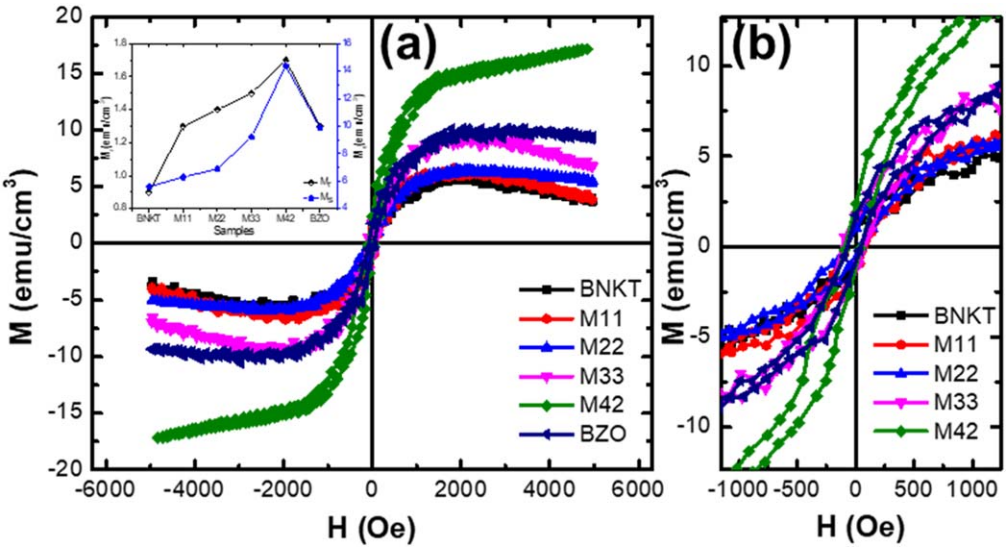

Fig. 4. (a) Room temperature magnetic hysteresis loops (*M–H*) for BNKT/BZO films under a magnetic field from −5 kOe to 5 kOe. (b) Magnetization of BNKT/BZO films focused in low magnetic fields from −1000 Oe to 1000 Oe. The insert shows differences in the M_s and M_r values between the heterolayered films.

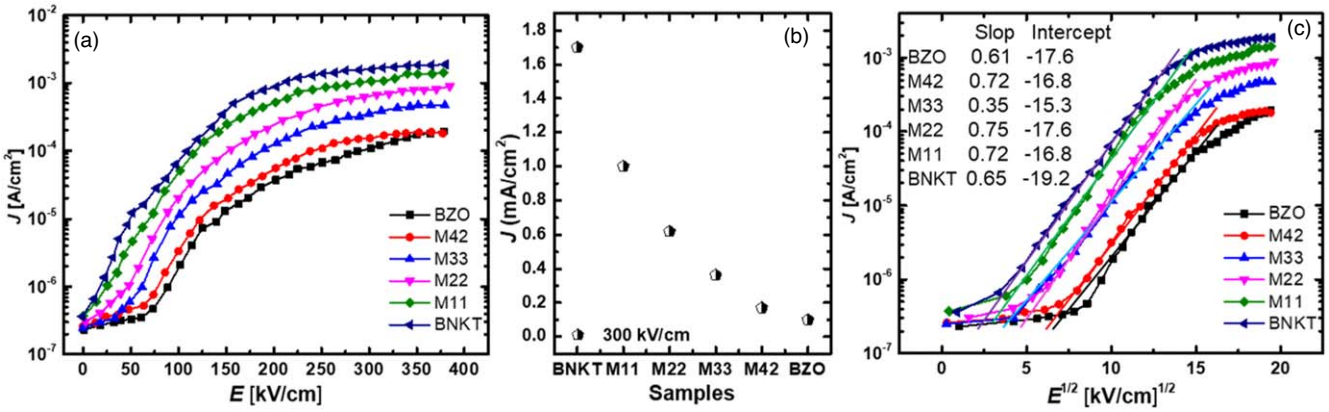

Fig. 5. (a) Dependence of leakage current density (J) on electric field E for the BNKT/BZO heterostructure films. (b) J values of heterostructure films measured at an electric field of 300 kV cm^{-1}. (c) Leakage current density represented as a function of the square root ($E^{1/2}$) of the field.

the leakage current is governed by the defect density in film layers. For heterolayered films, the BZO layer prevents the evaporation of Bi^{3+}, Na^{+} and K^{+} ions in BNKT layers during sintering at high temperature. For M42 film, the BZO layer coated on the top of the sample prevented metal ion evaporation; this was followed by a decline in oxygen vacancies and an enhancement of the electric properties.

The principle of $J(E)$ dependence can provide information about the possible conduction mechanisms in the heterolayered films. For example, a dependence type such as $J \sim E^2$, is responsible for a space charge-limited conduction (SCLC) mechanism.[34,35] Or another one, $\ln(J) \sim -(1/kT)(\Phi - aE^{1/2})$, where k is the Boltzmann constant, Φ is the height of the Schottky barrier and a is a material constant, is related to a Schottky-type conduction mechanism,[35] contributed by the potential barrier caused by the difference in Fermi level between the dielectric film and metal electrode. We investigated the obtained J data as a function of E^2 or $E^{1/2}$ on a logarithmic scale to determine the conduction mechanisms in the films. Figure 5(c) shows the J (in logarithmic scale) versus $E^{1/2}$ curve. For a standard Schottky emission, the plot of $\log(J)$ versus $E^{1/2}$ should be linear. This obviously expresses that J obeys the mechanism of a Schottky barrier in almost all the field range. The barrier height can be obtained from the intercept of the Schottky plot. The insert in Fig. 5(c) presents the intercepts and slopes obtained from fitted $\log(J)$–$E^{1/2}$ curves. The extracted Schottky barrier height between the Pt substrate and the film fluctuates from 0.80 eV to 0.92 eV.

The influence of different heterostructures on the microstructure, electric and magnetic properties of the BNKT/BZO heterolayered films has been reported in detail. The heterostructures are attributed to correlate to a enhancement of magnetic properties and leakage current density (J) of the films. For heterolayered M42 films, M_s and M_r reach the highest values of 14.4 emu cm^{-3} and 1.7 emu cm^{-3}, respectively, about three times higher than those of multilayered BNKT. The magnetic improvement is related to the magnetic interface effect caused by strongly correlated electron systems in BNKT and BZO layers in BNKT/BZO heterostructures. J decreases strongly from 16.0×10^{-4} A cm^{-2} for BNKT films to 1.4×10^{-4} A cm^{-2} for heterolayered M42 films. It is attributed that the decrease of J is derived by each interface restricting the probability that a potential leakage path reaches the outer electrodes. Another reason is that the BZO layer prevents the evaporation of metal ions in the BNKT layers during sintering at high temperatures, followed by a decline in oxygen vacancies, and an enhancement of electric properties. The Schottky barrier height between Pt substrate and film that was defined based on fitted $\log(J)$–$E^{1/2}$ curves fluctuates from 0.80 eV to 0.92 eV.

Acknowledgments This research is funded by Hanoi University of Science and Technology (HUST) under project No. T2021-PC-027.

ORCID iDs Ngo Duc Quan https://orcid.org/0000-0001-5654-7134

1) C.-W. Nan, M. I. Bichurin, S. Dong, D. Viehland, and G. Srinivasan, J. Appl. Phys. **103**, 031101 (2008).
2) E. Ascher, H. Rieder, H. Schmid, and H. Stössel, J. Appl. Phys. **37**, 1404 (1966).
3) J. Wang et al., Science **299**, 1719 (2003).
4) T. Kimura, T. Goto, H. Shintani, K. Ishizaka, T. Arima, and Y. Tokura, Nature **426**, 55 (2003).
5) N. Hur, S. Park, P. A. Sharma, J. S. Ahn, S. Guha, and S. W. Cheong, Nature **429**, 392 (2004).
6) Z. Hu et al., Sci. Rep. **6**, 32408 (2016).
7) R. Gao et al., Adv. Electron. Mater. **4**, 1800030 (2018).
8) R. Gao, Q. Zhang, Z. Xu, Z. Wang, W. Cai, G. Chen, X. Deng, X. Cao, X. Luo, and C. Fu, Nanoscale. **10**, 11750 (2018).
9) R. Gao, Q. Zhang, Z. Xu, Z. Wang, G. Chen, X. Deng, C. Fu, and W. Cai, Compos. B: Eng. **166**, 204 (2019).
10) B. Y. Wang et al., RSC Adv. **3**, 7884 (2013).
11) N. D. Quan, L. Huu Bac, D. V. Thiet, V. N. Hung, and D. D. Dung, Adv. Mater. Sci. Eng. **2014**, 1 (2014).
12) W. Jo, R. Dittmer, M. Acosta, J. Zang, C. Groh, E. Sapper, K. Wang, and J. Rödel, J. Electroceramics **29**, 71 (2012).
13) N. D. Quan, V. N. Hung, and D. D. Dung, J. Electron. Mater. **46**, 5814 (2017).
14) R. E. Eitel, C. A. Randall, T. R. Shrout, P. W. Rehrig, W. Hackenberger, and S.-E. Park, J. Appl. Phys. **40**, 5999 (2001).
15) Y. Hiruma, T. Watanabe, H. Nagata, and T. Takenaka, Jpn. J. Appl. Phys. **47**, 7659 (2008).
16) Y. Wang, G. Xu, X. Ji, Z. Ren, W. Weng, P. Du, G. Shen, and G. Han, J. Alloys Compd. **475**, L25 (2009).
17) N. A. Hill, J. Phys. Chem. B **104**, 6694 (2000).
18) N. D. Quan, N. D. Minh, and G. Rijnders, Jpn. J. Appl. Phys. **60**, 010902 (2021).
19) S. Lopatin, I. Lopatina, and I. Lisnevskaya, Ferroelectrics **162**, 63 (1994).
20) M. I. Bichurin, I. A. Kornev, V. M. Petrov, and I. V. Lisnevskaya, Ferroelectrics **204**, 289 (1997).
21) R. Ramesh and N. A. Spaldin, Nat. Mater. **6**, 21 (2007).
22) N. D. Quan, V. N. Hung, and D. D. Dung, Mater. Res. Express **4**, 086401 (2017).

23) L. Tong, H. Li, W. Ni, Y. Guo, Q. Li, H. Wang, and C. Wang, RSC Adv. **7**, 33708 (2017).
24) G. O. Jones and P. A. Thomas, Acta Crystallogr. Sec. B: Struct. Sci. **56**, 426 (2000).
25) N. T. Hung, L. H. Bac, N. N. Trung, N. T. Hoang, P. Van Vinh, and D. D. Dung, J. Magn. Magn. Mater. **451**, 183 (2018).
26) L. T. H. Thanh, N. B. Doan, L. H. Bac, D. V. Thiet, S. Cho, P. Q. Bao, and D. D. Dung, Mater. Lett. **186**, 239 (2017).
27) D. E.-S. Bakeer, A.-H. Sakr, H. A. Motaweh, and W. El-Sokary, J Nanostruct. **9**, 414 (2019).
28) P. P. Khirade, S. D. Birajdar, A. B. Shinde, and K. M. Jadhav, J. Alloys Compd. **691**, 287 (2017).
29) G. KH, L. ZQ, L. XJ, S. W, L. H, and J. EY, Solid State Commun. **138**, 175178 (2006).
30) J. Dho and X. D. Zhang, J. Korean Phys. Soc. **56**, 383 (2010).
31) S. Koohfar, A. B. Georgescu, A. N. Penn, J. M. LeBeau, E. Arenholz, and D. P. Kumah, npj Quantum Mater. **4**, 25 (2019).
32) R. Guo, H. Luo, M. Yan, X. Zhou, K. Zhou, and D. Zhang, Nano Energy. **79**, 105412 (2021).
33) M. D. Nguyen, Y. A. Birkhölzer, E. P. Houwman, G. Koster, and G. Rijnders, Adv. Energy Mater. **12**, 2200517 (2022).
34) S. J. Wang, S. Miao, I. M. Reaney, M. O. Lai, and L. Lu, J. Appl. Phys. **107**, 104104 (2010).
35) G. W. Pabst, L. W. Martin, Y.-H. Chu, and R. Ramesh, Appl. Phys. Lett. **90**, 072902 (2007).